

Hyperboloidal layers for hyperbolic equations on unbounded domains

Anıl Zenginoğlu

*Laboratoire Jacques-Louis Lions,
Université Pierre et Marie Curie (Paris 6), Paris, France*

Abstract

We show how to solve hyperbolic equations numerically on unbounded domains by means of compactification, thereby avoiding the introduction of an artificial outer boundary. The essential ingredient is a suitable transformation of the time coordinate in combination with compactification. Based on this idea, we present a new layer method, called hyperboloidal layers. Accuracy and efficiency of this method is demonstrated by numerical tests including the one dimensional Maxwell equations using finite difference methods, and the three dimensional scalar wave equation with and without nonlinear source terms using spectral methods.

Keywords: Transparent (non-reflecting, absorbing) boundary conditions, perfectly matched layers, hyperboloidal layers, hyperboloidal compactification, wave equations, Maxwell equations.

1. Introduction

Hyperbolic equations typically admit wave-like solutions that oscillate infinitely many times in an unbounded domain. Take a plane wave in one space dimension with frequency ω and wave number k

$$u(x, t) = e^{2\pi i(kx - \omega t)}. \quad (1)$$

Any mapping of such an oscillatory solution from an infinite domain to a finite domain will result in infinitely many oscillations near the domain boundary, which cannot be resolved numerically. We refer to this phenomenon as the compactification problem. It is commonly stated that hyperbolic partial differential equations are not compatible with compactification, and therefore can not be solved on unbounded domains accurately.

One can, however, perform a transformation of the *time coordinate* such that there are only a finite number of oscillations in an infinitely extended spatial domain. Introduce

$$\tau(x, t) = t - \frac{k}{\omega} \left(x + \frac{C}{1+x} \right), \quad (2)$$

where C is a finite, positive constant. The plane wave (1) becomes

$$u(x, \tau) = e^{-2\pi i(kC/(1+x) + \omega\tau)}. \quad (3)$$

This representation of the plane wave has only kC cycles along a constant time hypersurface in the unbounded spatial domain $x \in [0, \infty)$, and is therefore compatible with compactification.

The simple idea just described has far reaching consequences. In numerical calculations of hyperbolic equations one typically truncates the unbounded solution domain by introducing an artificial outer boundary that is not part of the original problem. Boundary conditions – called transparent, absorbing, radiative, or non-reflecting – are constructed to simulate transparency of this artificial outer boundary. There has been significant developments in the treatment of artificial outer boundaries since the 70's, but there is no consensus on optimal treatment [1, 2]. Especially the construction of boundary conditions for nonlinear problems is difficult [3]. A successful technique for numerical calculations on unbounded domains resolves this problem for certain hyperbolic systems, besides giving direct quantitative access to asymptotic properties of solutions.

Furthermore, the numerical construction of oscillatory solutions of the type (3) can be very efficient. Numerical accuracy requirements for hyperbolic equations are typically given in terms of numbers of grid points per wavelength. In the example presented above, we have at our disposal the parameter C that determines the number of cycles to be resolved, which can be chosen to be small. This suggests that high order numerical discretizations requiring a few points per wavelength can be very efficient in combination with time transformations of the type (2).

The rest of the paper is devoted to the discussion of time transformation and compactification for hyperbolic equations. The theoretical part of the paper (sections 2 and 3) presents the method in detail. We describe the compactification problem (section 2.1) and its resolution (section 2.2) for the advection equation in one dimension. In section 2.3 we discuss the more interesting case with incoming and outgoing characteristics for the wave equation. We show that the method works also for systems of equations (section 2.4). Compactifying layers are introduced in section 2.5 in analogy to absorbing layers. The layer strategy allows us to employ arbitrary coordinates in an inner domain, where scatterers or sources may be present. In spatial dimensions more than one, compactification is performed in the outgoing direction in combination with rescaling to take care of the asymptotic fall off behavior (sections 3.1 and 3.2). We finish the theoretical part discussing possible generalizations of the method to non-spherical coordinate systems (section 3.3). Section 4 presents numerical experiments in one and three spatial dimensions. In one dimension, we solve the Maxwell equations using finite difference methods (section 4.1). A stringent test of the method is presented by taking off-centered initial data for the wave equation in three spatial dimensions with nonlinear source terms (section 4.2). We conclude with a discussion in section 5.

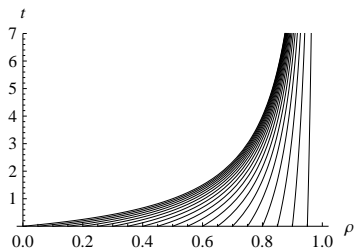


Figure 1: Characteristic diagram for the advection equation after spatial compactification. The characteristic speed approaches zero near spatial infinity at $\{\rho = 1\}$ causing loss of numerical resolution: this is the compactification problem.

2. Compactification in one spatial dimension

2.1. Spatial compactification

Consider the initial boundary value problem for the advection equation

$$\partial_t u + \partial_x u = 0, \quad u(x, 0) = u_0(x), \quad u(0, t) = b(t). \quad (4)$$

The problem is posed on the unbounded domain $x \in [0, \infty)$. We transform the infinite domain in x to a finite domain by introducing the compactifying coordinate ρ via

$$\rho(x) = \frac{x}{1+x}, \quad x(\rho) = \frac{\rho}{1-\rho}. \quad (5)$$

The advection equation becomes

$$\partial_t u + (1-\rho)^2 \partial_\rho u = 0. \quad (6)$$

The spatial domain is now given by $\rho \in [0, 1]$. Characteristics of this equation are solutions to the ordinary differential equation

$$\frac{d\rho(t)}{dt} = -(1-\rho(t))^2.$$

They are plotted in figure 1. The compactification problem is clearly visible: the coordinate speed of characteristics approaches zero near a neighborhood of the point that corresponds to spatial infinity. The intuitive reason for this behavior is that the advection equation has a finite speed of propagation and therefore its characteristics cannot reach infinity in a finite time.

A concrete example illustrates the problem for oscillatory solutions. Set initial data $u_0(x) = \sin(2\pi x)$ and boundary data $b(t) = -\sin(2\pi t)$ in (4). We obtain the solution

$$u(x, t) = \sin(2\pi(x - t)), \quad (7)$$

which reads in the compactifying coordinate (5)

$$u(\rho, t) = \sin\left(2\pi\left(\frac{\rho}{1-\rho} - t\right)\right). \quad (8)$$

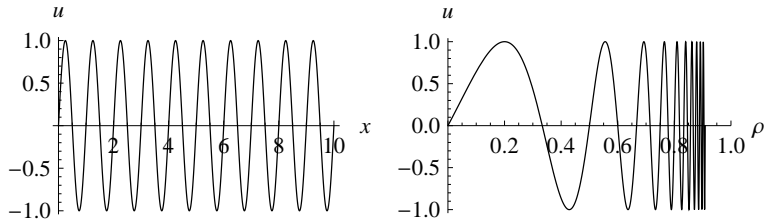


Figure 2: The solution (7) at time $t = 0$ is plotted on the left panel. The same solution in the compactifying coordinate given in (8) plotted on the right panel illustrates infinite blueshift in frequency.

The solution is depicted in figure 2 at $t = 0$ on the domain $x \in [0, 10]$ in the original coordinate and on the domain $\rho \in [0, 10/11]$ in the compactifying coordinate. The oscillations cannot be resolved in the compactifying coordinate near infinity due to infinite blueshift in spatial frequency.

It seems that the price of mapping infinity to a finite coordinate distance is the requirement of infinite resolution. However, a suitable time transformation as discussed in the next section provides a clean solution to this problem.

2.2. Hyperboloidal compactification

The idea is to perform a transformation of the time coordinate as in (2). We introduce

$$\tau = t - \left(x + \frac{C}{1+x} \right), \quad (9)$$

With the compactification (5) we get the Jacobian

$$\partial_\tau = \partial_t, \quad \partial_x = (-1 + C\Omega^2)\partial_\tau + \Omega^2\partial_\rho,$$

where we defined $\Omega = 1 - \rho$. The advection equation in the new coordinates (ρ, τ) reads

$$\partial_\tau u + \frac{1}{C}\partial_\rho u = 0.$$

This equation has the same form, up to an additional free parameter, as the advection equation in the original coordinates (4), but the meaning of the coordinates is different. Solutions to the above equation in the bounded domain $\rho \in [0, 1]$ correspond to solutions to the original advection equation in the unbounded domain $x \in [0, \infty)$. The free parameter C expresses the freedom in the time transformation to prescribe the characteristic speeds in the compactifying coordinates and the number of cycles in an infinite domain. To see this we write the solution (7) in the new compactifying coordinates

$$u(\rho, \tau) = -\sin(2\pi(C\Omega + \tau)). \quad (10)$$

The solution is depicted in figure 3 at $\tau = 0$ for two values of C . The number of cycles on the solution domain depends on C . We remark that surfaces of constant τ do not correspond to surfaces of constant t .

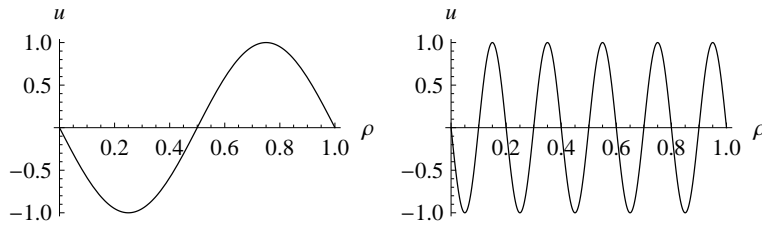


Figure 3: The solution (10) at time $\tau = 1$ is plotted for two values of C . On the left panel we have $C = 1$ and on the right panel $C = 5$. The number of oscillations, and therefore the wavelength of the solution, can be influenced by the free parameter C .

The idea to introduce a coordinate transformation of time in combination with compactification comes from general relativity [4]. The time function (2) has the property that, asymptotically, it resembles characteristics of the advection equation. Infinity along characteristic directions is referred to as null infinity. Time functions whose level sets approach null infinity are called *hyperboloidal* because their asymptotic behavior is similar to the asymptotic behavior of standard hyperboloids [5]. To see this, consider the rectangular hyperbola on the (x, t) plane, $t^2 - x^2 = C^2$, with a free parameter C . Shifting the hyperbola along the t direction by τ gives $(t - \tau)^2 - x^2 = C^2$. Introducing τ as the new time coordinate we write

$$\tau(x, t) = t - \sqrt{C^2 + x^2}. \quad (11)$$

We plot in figure 4 two families of hyperbolae with $C = 1$ and $C = 5$. The asymptotes of these hyperbolae on $x > 0$ are the characteristics of the advection equation, $\tau = t - x$, for any value of C . This is the same asymptotic behavior as that of (9), hence the name hyperboloidal for such time functions. A suitable compactification along level sets of such time functions sets the coordinate location of null infinity to a time independent value (see [6] for a discussion of conformal and causal properties of hyperboloidal time functions and compactification on asymptotically flat spacetimes).

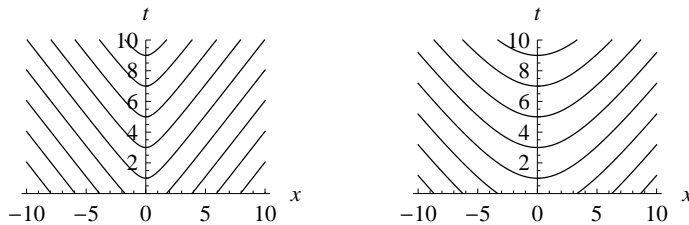


Figure 4: Rectangular hyperbola (11) for $C = 1$ and $C = 5$ depicted on the (x, t) plane. The hyperbolae are flatter near the origin for larger C but their asymptotic behavior in leading order is independent of C .

It is useful to summarize the hyperboloidal compactification technique with general expressions. We introduce coordinates ρ and τ via

$$\tau = t - h(x), \quad x = \frac{\rho}{\Omega}. \quad (12)$$

The height function, h , must satisfy $dh/dx < 1$ so that τ is a time function. We also require that the gradient of the function $\Omega \equiv \Omega(\rho)$ is nonvanishing at its zero set. The zero set of Ω corresponds to infinity with respect to x . The coordinate transformations have the Jacobian

$$\partial_t = \partial_\tau, \quad \partial_x = -H \partial_\tau + \frac{\Omega^2}{L} \partial_\rho, \quad \text{where } H := \frac{dh}{dx}(\rho), \quad L := \Omega - \rho \frac{d\Omega}{d\rho}. \quad (13)$$

The advection equation becomes in this general notation

$$\partial_\tau u + \frac{\Omega^2}{(1-H)L} \partial_\rho u = 0. \quad (14)$$

The specific choices (5) and (9) satisfy

$$\frac{\Omega^2}{(1-H)L} = \frac{1}{C}. \quad (15)$$

In general, the time transformation must be chosen such that we have asymptotically in x , or equivalently as Ω approaches zero

$$1 - H \sim O(\Omega^2). \quad (16)$$

This relation expresses that the asymptotic heightening of time surfaces needs to be in the order of the compressing of space so that we have a uniform outgoing characteristic speed over an infinitely compressed domain. In light of this intuition, we refer to H as the heighten function, and to Ω as the compress function.

2.3. Wave equation

The advection equation discussed in the previous section is a special example because its characteristics propagate in only one direction. A more representative example for hyperbolic partial differential equations is the wave equation, which has both incoming and outgoing characteristics. The wave equation reads in standard coordinates

$$\partial_t^2 u - \partial_x^2 u = 0. \quad (17)$$

Its characteristics on a bounded domain are plotted on the left panel of figure 5. We are interested in the problem on the unbounded domain $x \in (-\infty, \infty)$. With (13) we get

$$\left[\partial_\tau^2 + \frac{\Omega^2}{(1-H^2)L} \left(2H \partial_\tau \partial_\rho - \frac{\Omega^2}{L} \partial_\rho^2 + \partial_\rho(H) \partial_\tau - \partial_\rho \left(\frac{\Omega^2}{L} \right) \partial_\rho \right) \right] u = 0. \quad (18)$$

The transformation (9) is not the right choice for this case. Instead, we choose the height function of standard hyperboloids, $h(x) = \sqrt{C^2 + x^2}$. We wish to have the freedom for prescribing an arbitrary coordinate location for null infinity, which corresponds to the zero set of the compress function. We set

$$\Omega = \frac{S^2 - \rho^2}{2CS} \quad \Rightarrow \quad L = \frac{S^2 + \rho^2}{2CS} \quad \text{and} \quad H = \frac{2S\rho}{S^2 + \rho^2}. \quad (19)$$

The parameter S determines the coordinate location of null infinity on the numerical grid. The unbounded domain $x \in (-\infty, \infty)$ corresponds in the compactifying coordinate to $\rho \in (-S, S)$. The wave equation becomes

$$\partial_\tau^2 u + \frac{2\rho}{C} \partial_\tau \partial_\rho u - \Omega^2 \partial_\rho^2 u + \frac{2S\Omega}{S^2 + \rho^2} \partial_\tau u + \frac{(3S^2 + \rho^2)\rho\Omega}{SC(S^2 + \rho^2)} \partial_\rho u = 0. \quad (20)$$

The equation evaluated at infinity, $\{\rho = \pm S\}$, takes the form

$$\partial_\tau \left(\partial_\tau \pm \frac{2S}{C} \partial_\rho \right) u = 0,$$

reflecting that both boundaries are outflow boundaries and do not require boundary conditions.

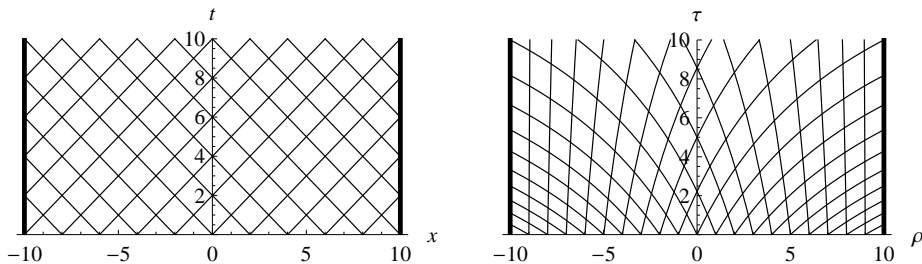


Figure 5: On the left panel we plot the characteristics for the standard wave equation (17) on the bounded domain $x \in [-10, 10]$. On the right panel hyperboloidal compactification has been applied with infinity located at $\rho = S = \pm 10$, and $C = 10$. The standard wave equation on a bounded domain requires boundary conditions for the incoming characteristics from both boundaries. With hyperboloidal compactification there are no incoming characteristics, and the coordinate speed of outgoing characteristics can be controlled by the free parameter C .

The characteristics of the wave equation (20) are plotted on the right panel of figure 5. No boundary conditions are needed because no characteristics enter the simulation domain. Furthermore, the outgoing characteristics leave the domain smoothly through the outflow boundaries.

The initial value problem for the wave equation (17) with data on a t surface is related to the initial value problem for (18) by time evolution of the equation as indicated in figure 4. This may be an undesired complication in practical applications. If one is interested in the evolution of certain compactly supported data, one may keep the t surfaces in an interior domain which includes the

data and apply hyperboloidal compactification only in the exterior domain as discussed in section 2.5.

The above calculation is made for the one dimensional, source free, constant coefficient wave equation. The method applies directly when variable coefficients or lower order terms are present. The requirement on the variable coefficients in the principal part is that they are asymptotically constant. For the lower order terms we require a fall off behavior of at least Ω^2 so that the division by $1 - H^2$ in (18) leads to a regular equation.

2.4. Hyperbolic systems

Consider the linear, homogeneous system of partial differential equations with variable coefficients

$$\partial_t \mathbf{u} = \mathbf{A} \partial_x \mathbf{u}, \quad (21)$$

where $\mathbf{u} = (u_1(x, t), u_2(x, t), \dots, u_n(x, t))^T$, and \mathbf{A} is an $n \times n$ matrix that may depend on x . The transformation (12) with Jacobian (13) leads to

$$(\mathbb{1} + H\mathbf{A})\partial_\tau \mathbf{u} = \frac{\Omega^2}{L} \mathbf{A} \partial_\rho \mathbf{u}. \quad (22)$$

Assuming that the time transformation has been chosen to satisfy (16), we require that the polynomial remainder of $\det(\mathbb{1} + H\mathbf{A})$ by $1 - H$ vanishes asymptotically. This is a condition on the asymptotic form of the elements of \mathbf{A} . For example, taking $n = 2$ we write

$$\mathbf{A} = \begin{pmatrix} a_{11} & a_{12} \\ a_{21} & a_{22} \end{pmatrix}.$$

The asymptotic condition for the applicability of hyperboloidal compactification reads

$$1 + a_{11} + a_{22} - a_{12}a_{21} + a_{11}a_{22} = 0. \quad (23)$$

A typical example is the wave equation (17) written as a first order symmetric hyperbolic system. The wave equation takes the form (21) in the auxiliary variables $v = \partial_t u$ and $w = \partial_x u$, with

$$\mathbf{u} = \begin{pmatrix} v \\ w \end{pmatrix}, \quad \mathbf{A} = \begin{pmatrix} 0 & 1 \\ 1 & 0 \end{pmatrix}. \quad (24)$$

The condition (23) is satisfied. The transformed system reads

$$\partial_\tau \mathbf{u} = \frac{\Omega^2}{(1 - H^2)L} \begin{pmatrix} -H & 1 \\ 1 & -H \end{pmatrix} \partial_\rho \mathbf{u}. \quad (25)$$

The particular choice (19) leads to the regular system

$$\partial_\tau \mathbf{u} = \frac{1}{2CS} \begin{pmatrix} -2S\rho & S^2 + \rho^2 \\ S^2 + \rho^2 & -2S\rho \end{pmatrix} \partial_\rho \mathbf{u}.$$

The outer boundaries of this system at $\rho = \pm S$ are pure outflow boundaries.

As a further example consider the one dimensional Maxwell equations for the electric and magnetic fields (\bar{E}, \bar{H})

$$\partial_t \bar{E} = -\frac{1}{\epsilon} \partial_x \bar{H}, \quad \partial_t \bar{H} = -\frac{1}{\mu} \partial_x \bar{E},$$

The electric permittivity ϵ and the magnetic permeability μ may be point-dependent. The equations have the form (21) with

$$\mathbf{u} = \begin{pmatrix} \bar{E} \\ \bar{H} \end{pmatrix}, \quad \text{and} \quad \mathbf{A} = -\frac{1}{\epsilon\mu} \begin{pmatrix} 0 & \mu \\ \epsilon & 0 \end{pmatrix}.$$

We get after applying hyperboloidal compactification

$$\partial_\tau \mathbf{u} = -\frac{\Omega^2}{(\epsilon\mu - H^2)L} \begin{pmatrix} H & \mu \\ \epsilon & H \end{pmatrix} \partial_\rho \mathbf{u}. \quad (26)$$

In vacuum outside a compact domain we have $\epsilon = \epsilon_0$ and $\mu = \mu_0$ where ϵ_0 and μ_0 are the electric and the magnetic constants. We need to choose the asymptotic behavior of H such that $\sqrt{\epsilon_0\mu_0} - H \sim O(\Omega^2)$. Then the Maxwell equations behave similarly to the wave equation (25) near null infinity.

The example of Maxwell equations suggests that including lower order terms or variable characteristic speeds in a compact domain are straightforward in the hyperboloidal method as long as the asymptotic form of the equations are suitable. The asymptotic characteristic speeds need to be constant and lower order terms need to have compact support or fall off sufficiently fast. In the next section we discuss how hyperboloidal compactification can be restricted to a layer attached to an interior domain.

2.5. Hyperboloidal layers

It may be desirable to employ a specific coordinate system in a compact domain without the time transformation or the compactification required by the hyperboloidal method. One reason is technical. Elaborate numerical techniques to deal with shocks, scatterers, and media assume predominantly a specific coordinate system. It may be impractical to modify these methods to work with hyperboloidal compactification throughout the simulation domain. Another reason is initial data. One may be interested in the evolution of certain (compactly supported) initial data prescribed on a level set of t . In these cases it may be favourable to restrict the hyperboloidal compactification to a layer.

We discuss briefly the perfectly matched layer (PML) by Bérenger [7] to set the stage for hyperboloidal layers. In the PML method one attaches an absorbing medium – a layer – to the domain of interest such that the interface between the interior domain and the exterior medium is transparent independent from the frequency and the angle of incidence of the outgoing wave. Inside the layer the solution decays exponentially in the direction normal to the interface. As a consequence the solution is close to zero at the outer boundary of the layer where any stable boundary condition may be applied. The reflections from the outer boundary can be ignored if the layer is sufficiently wide.

The success of the PML method lies in the transparency of the interface between the interior domain and the layer. This property finds explanation in the interpretation of Chew and Weedon of the PML as the analytic continuation of the equations into complex coordinates [8]. The challenge is then to find suitable choices of the equations and the free parameters that lead to exponential damping of the solution in a stable way, which may be difficult depending on the system [9, 10, 11].

A simple example, omitting details of the method beyond our needs, demonstrates the basic idea. We perform an analytic continuation of x into complex coordinates beyond a certain interface R . Then the coordinate x can be written in terms of its real and imaginary parts as $\text{Re}(x) + i\sigma\text{Im}(x)\Theta(x - R)$, where σ is a positive parameter, and Θ denotes the Heaviside step function. Setting $k = 1$, the plane wave (1) at time $t = 0$ becomes

$$u(x, 0) = e^{2\pi i \text{Re}(x)} e^{-2\pi \sigma \text{Im}(x) \Theta(x - R)}. \quad (27)$$

The strength of the exponential decay is controlled by a free parameter σ . The solution is plotted in figure 6 for $\sigma = 0.1$.

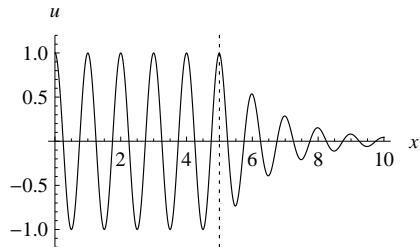


Figure 6: The plane wave solution with the spatial coordinate analytically extended into the complex plane (27) demonstrates how outgoing waves are damped exponentially in the absorbing layer of the PML method. We set $\sigma = 0.1$ and $R = 5$. The dashed line indicates the location of the interface.

For a hyperboloidal layer we perform a real coordinate transformation, both of space and time, beyond a certain timelike surface $x = R$, which we refer to as the interface. We set

$$x - R = \frac{\rho - R}{\Omega}, \quad \Omega = 1 - \frac{(\rho - R)^2}{(S - R)^2} \Theta(\rho - R), \quad (28)$$

where the coordinate location of infinity satisfies $S > R$. The width of the layer is $S - R$. The coordinates x and ρ coincide up to second order along the interface.

A simple prescription for the heighten function can be obtained by requiring that the outgoing characteristic speed is unity across the layer. For example, the outgoing and incoming characteristic speeds c_{\pm} for the wave equation on $\rho > 0$ are

$$c_{\pm} = \frac{\Omega^2}{L(\pm 1 - H)}, \quad \text{with} \quad L = \Omega - (\rho - R) \frac{d\Omega}{d\rho}. \quad (29)$$

The requirement of unit outgoing characteristic speed reads $c_+ = 1$, implying

$$1 - H = \frac{\Omega^2}{L}. \quad (30)$$

For $\rho < -R$ we require $c_- = -1$. The resulting characteristics are depicted in figure 7. For $|\rho| < R$ we obtain the standard characteristics in (x, t) coordinates. For $|\rho| > R$ we obtain the hyperboloidal characteristics in (ρ, τ) coordinates (compare figure 5). No characteristics enter the computational domain.

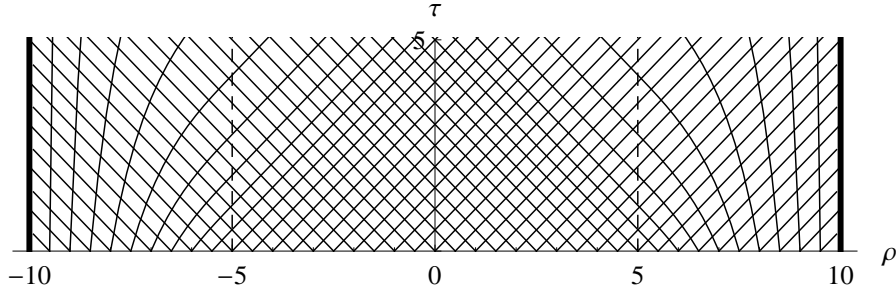


Figure 7: Characteristic structure for hyperboloidal layers with boundaries located at $\rho = \pm S = \pm 10$ and interfaces at $\rho = \pm R = \pm 5$. Compare the inner domain $[-5, 5]$ to the left panel of figure 5, and the layers $[-10, -5]$ and $[5, 10]$ to the right panel of figure 5.

The plane wave in the layer has the same form as in the interior under these choices. It has been depicted on figure 8, where the dashed line indicates the location of the interface. The important difference to the standard case is that the incoming characteristic speed vanishes at the outer grid boundary.

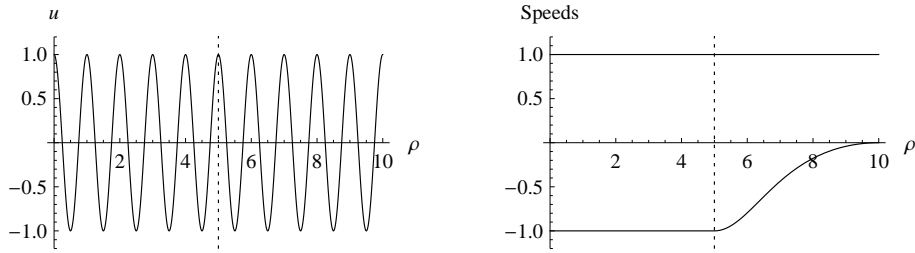


Figure 8: On the left panel we plot the plane wave solution with the compress function given in (28) and the heighten function given in (30). The characteristic speeds are depicted on the right panel in which the top and the bottom curves correspond to outgoing and incoming characteristic speeds. The domain is given by $\rho \in [0, 10]$ with a compactifying layer starting at $\rho = R = 5$ as indicated by the dashed lines. The incoming characteristic speed at the outer boundary vanishes, therefore no outer boundary conditions are needed in the layer.

There is a large freedom in the choices of compress and heighten functions, which can be exploited for specific purposes. As an example, take a linear compress function

$$\Omega = 1 - \frac{\rho - R}{S - R} \Theta(\rho - R), \quad (31)$$

and use the heighten function of standard hyperboloids translated by R

$$H = \frac{x - R}{\sqrt{(x - R)^2 + C^2}} \Theta(x - R). \quad (32)$$

The resulting representation of the plane wave is plotted on the left panel of figure 9 for $C = 3$. In this case we have fewer oscillations in the layer than in the interior because of the spatial redshift controlled by C . A strong redshift, and consequently few spatial oscillations, may be preferable in a high order spatial discretization scheme in which a few grid points per wavelength are sufficient for good accuracy. On the right panel of figure 9, however, we see that strong spatial redshift comes at a price: the outgoing coordinate speed increases strongly in the layer. Evaluation of c_+ from (29) at infinity with our current choices gives $c_+ = 2(S - R)^2/C^2$. A small value for C with a wide layer leads to a high outgoing characteristic speed, which requires small time steps in an explicit time stepping algorithm. The balance between the accuracy in time and in space can be influenced by the compress and heighten functions, and the free parameters included in them. The specific choices will depend on the requirements of the problem. It can be expected that in most cases the outgoing characteristic speed in the layer will be chosen equal to the speed in the interior domain as in figure 8.

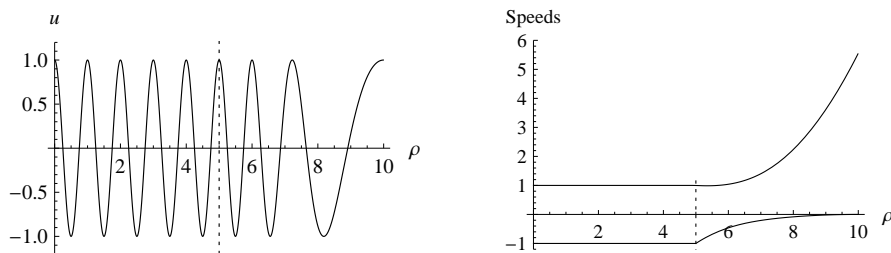


Figure 9: On the left we plot the plane wave solution with (31) and (32) for $C = 3$ in the otherwise same setting as in figure 8. There are fewer oscillations in the layer due to the stronger redshift causing a higher outgoing characteristic speed as depicted on the right panel.

The compactifying layer is similar to the PML in that both methods allow us to solve the equations of interest in standard coordinates in an inner domain. In both cases the interface between the inner domain and the layer is transparent on the analytical level, independent of the frequency and angle of incidence of the outgoing wave. The key difference is that the PML absorbs the outgoing wave so that it is damped exponentially, whereas the compactifying layer transports it to infinity. The solution in the hyperboloidal layer is of interest, as opposed to the solution in the absorbing layer. In fact, the solution at the outer boundary of the layer is of great interest in radiative systems because it gives the radiation signal as observed by an idealized observer at infinity.

3. Multiple dimensions

Hyperboloidal compactification is directly applicable in multiple dimensions when compactification is performed in the outgoing direction. The main difference in multiple dimensions is that a rescaling of the unknown fields needs to be performed such that the fields attain a non-vanishing finite limit at infinity. The rescaling depends on the fall off behavior of these fields, and therefore on the equation and the dimension of the problem.

3.1. Rescaling

We begin our discussion with the three dimensional wave equation on flat space

$$\left(-\partial_t^2 + \Delta_{\mathbb{R}^3}\right) u = 0.$$

Here, $\Delta_{\mathbb{R}^3}$ is the Laplace operator on the three dimensional Euclidean space. We write the wave equation in spherical coordinates to single out the outgoing direction

$$\left(-\partial_t^2 + \partial_r^2 + \frac{1}{r}\partial_r + \frac{1}{r^2}\Delta_{\mathbb{S}^2}\right) u = 0,$$

with $\Delta_{\mathbb{S}^2}$ as the Laplace-Beltrami operator on the two sphere. In section 2.3 we showed that hyperboloidal compactification introduces a divisor that is proportional to the square of the compress function. With the compactification $r = \rho/\Omega$ we see that any term beyond the flat wave operator on the (r, t) plane that falls off as r^{-2} or faster is multiplied with at least Ω^2 , and is therefore regular under hyperboloidal compactification.

The angular part of the wave equation in spherical coordinates admits a regular compactification. The first radial derivative term, however, results in a singular operator at infinity as a straightforward calculation shows. We resolve this problem by rescaling. It is well known that the three dimensional wave equation on the (r, t) plane takes the form of the one dimensional wave equation in the rescaled variable $v := ru$. We get

$$\left(-\partial_t^2 + \partial_r^2 + \frac{1}{r^2}\Delta_{\mathbb{S}^2}\right) v = 0,$$

which admits a regular hyperboloidal compactification.

This procedure generalizes to dimensions other than three. The essential feature of the rescaling is that it takes care of the fall off behavior of the scalar field: in three dimensions ru attains a regular limit at infinity. In n dimensions, the rescaling depends on n . Solutions to the wave equation decay asymptotically as $r^{-(n-1)/2}$ due to energy conservation. We expect therefore that the n dimensional wave equation written for the rescaled variable $v := r^{(n-1)/2}u$, admits a regular hyperboloidal compactification.

The n dimensional wave equation in spherical coordinates reads

$$\left(-\partial_t^2 + \partial_r^2 + \frac{n-1}{r}\partial_r + \frac{1}{r^2}\Delta_{\mathbb{S}^{n-1}}\right) u = 0,$$

where $\Delta_{\mathbb{S}^{n-1}}$ is the Laplace-Beltrami operator on the $n-1$ sphere. Transforming to the rescaled variable $v := r^{(n-1)/2}u$, we get

$$\left(-\partial_t^2 + \partial_r^2 - \frac{1}{4r^2}(n-1)(n-3) + \frac{1}{r^2}\Delta_{\mathbb{S}^{n-1}}\right)v = 0.$$

All terms beyond the one dimensional wave operator fall off as r^{-2} and are therefore amenable to a regular hyperboloidal compactification.

The inclusion of sources or of suitable nonlinearities is straightforward under the condition that the corresponding terms in the equation fall off sufficiently fast. For example, a power nonlinearity on the right hand side of the wave equation of the type u^p leads to the forcing term $v^p r^{-(n-1)(p-1)/2}$. This term is regular under hyperboloidal compactification if the power of r is -2 or lower, which implies $p \geq 1 + 4/(n-1)$. The critical power for which equality is satisfied is also the critical conformal power for semilinear wave equations with a power nonlinearity. This is not a coincidence as explained in the next section.

3.2. Conformal method

Compactification of spacetimes with a suitable time transformation as proposed by Penrose in [4] as well the hyperboloidal initial value problem as proposed by Friedrich [5] employ conformal methods. The conformal language is prevalent in studies of spacetimes in general relativity [12]. In this section we discuss the hyperboloidal compactification from the point of view of conformal techniques. This viewpoint is of theoretical and practical interest because it reveals the interplay of conformal geometry, partial differential equations, and numerical methods within the hyperboloidal approach, and also simplifies the implementation of the method in certain cases. We emphasize, however, that hyperboloidal compactification is independent of the conformal language.

In general, a hyperboloidal time transformation with a spatial compactification leads to a singular metric. Consider the Minkowski metric in spherical coordinates

$$\eta = -dt^2 + r^2 dr^2 + r^2 d\sigma^2, \quad (33)$$

where $d\sigma^2$ is the standard metric on the unit sphere. Introducing new coordinates τ and ρ as in (12) gives [6]

$$\eta = -d\tau^2 - \frac{2HL}{\Omega^2}d\tau d\rho + \frac{1-H^2}{\Omega^4}L^2 d\rho^2 + \frac{\rho^2}{\Omega^2}d\sigma^2.$$

This representation of the Minkowski metric is singular at infinity, but the singularity can be removed by conformally rescaling the metric to obtain

$$g = \Omega^2 \eta = -\Omega^2 d\tau^2 - 2HL d\tau d\rho + \frac{1-H^2}{\Omega^2}L^2 d\rho^2 + \rho^2 d\sigma^2. \quad (34)$$

The conformal metric g is regular at null infinity by (16), and can be extended beyond null infinity in a process referred to as conformal extension [4, 12, 13]. In this context, the function Ω is called the conformal factor. The zero set of

the conformal factor corresponds to null infinity where it has a non-vanishing gradient. These properties of the conformal factor lie behind our choices for the compress function in the previous sections.

Partial differential equations within the conformal framework have first been studied for fields with vanishing rest mass, such as scalar, electromagnetic, and gravitational fields [13]. The key observation is that the complicated asymptotic analysis of solutions to these partial differential equations can be replaced with local differential geometry by considering the conformally transformed equations in a conformally extended (regular) spacetime [14, 15].

We discuss the wave equation on Minkowski spacetime as an example for conformal methods. Under a conformal rescaling of the Minkowski metric, $g = \Omega^2 \eta$, the wave equation transforms as [12, 13]

$$\left(\square_g - \frac{n-1}{4n} R[g] \right) v = \Omega^{-(n+3)/2} \square_\eta u, \quad \text{with } v := \Omega^{(1-n)/2} u. \quad (35)$$

Here, $\square_g := g^{\mu\nu} \nabla_\mu \nabla_\nu$ is the d'Alembert operator with respect to g , $R[g]$ is the Ricci scalar of g , and n is the spatial dimension of the spacetime. We recognize the power of Ω that also appears in the definition of the rescaled variable v . This rescaling is asymptotically equivalent to the rescaling in section 3.1 where we factored out the fall off behavior of u such that the rescaled variable v has a non-vanishing limit at null infinity. To see this, consider a concrete choice for Ω that we made in previous sections, say $\Omega(\rho) = 1 - \rho$ as in (5). In terms of the coordinate $r = \rho/\Omega$, the conformal factor reads $\Omega(r) = (1+r)^{-1}$, which behaves asymptotically as r^{-1} . Therefore the definition of v in (35) corresponds asymptotically to the definition of v in section 3.1.

We can also explain the observation made at the end of section 3.1 concerning the agreement between the critical conformal power and the critical power for which hyperboloidal compactification leads to a regular equation. Using $\square_\eta u = u^p$ and the definition of v in (35) we get at the right hand side of the conformally invariant wave equation $\Omega^{((n-1)p-(n+3))/2} v^p$. For the regularity of this forcing term at infinity, where the conformal factor vanishes, we require $(n-1)p \geq n+3$, which is the same condition as in section 3.1. Equality is obtained for $p_c = 1 + 4/(n-1)$ for which the semilinear wave equation is conformally invariant, hence p_c is called the critical conformal power.

The conformal approach may be useful for various reasons. It extends directly to asymptotically flat backgrounds with non-vanishing curvature [6, 16]. It suggests a hyperboloidal layer in which the rescaling is performed with a conformal factor, or equivalently a compress function, such as (28). It also helps identifying the transformation behavior of the equations independent of coordinates. For example, Yang-Mills and Maxwell equations are conformally invariant, and therefore do not require a rescaling of the variables. Note, however, that the splitting of the equations or the specific variables in which the covariant equations are written may not be conformally invariant and may require a rescaling.

3.3. Non-spherical coordinate systems

It is straightforward to employ non-spherical coordinate systems in combination with hyperboloidal compactification if there is a unique outgoing direction. The outgoing direction is described by a coordinate that has closed coordinate surfaces. The reason behind this requirement is that cuts of null infinity are spheres.

An example that is useful especially in electromagnetism is given by prolate spheroidal coordinates. The relation between Cartesian coordinates $\{x, y, z\}$ and prolate spheroidal coordinates $\{\mu, \nu, \phi\}$ reads

$$x = \sinh \mu \sin \nu \cos \phi, \quad y = \sinh \mu \sin \nu \sin \phi, \quad z = \cosh \mu \cos \nu.$$

We have $r^2 = \sinh^2 \mu + \cos^2 \nu$. Here, μ is the outgoing direction that has closed coordinate surfaces. Compactification needs to be performed along μ . Using the conformal method, we argue that if conformal compactification of Minkowski spacetime in these coordinates leads to an explicitly regular metric, the equations that we solve on that background will be regular. The Minkowski metric reads

$$\eta = -dt^2 + dx^2 + dy^2 + dz^2 = -dt^2 + (\sinh^2 \mu + \sin^2 \nu) (d\mu^2 + d\nu^2) + \sinh^2 \mu \sin^2 \nu d\phi^2.$$

We introduce a new time coordinate by setting

$$\tau = t - \sqrt{1 + \sinh^2 \mu}.$$

The metric becomes

$$\eta = -d\tau^2 - 2 \sinh \mu d\mu d\tau + \sin^2 \nu d\mu^2 + (\sinh^2 \mu + \sin^2 \nu) d\nu^2 + \sinh^2 \mu \sin^2 \nu d\phi^2.$$

Compactification along the μ direction is performed via

$$\sinh \mu = \frac{2\rho}{1 - \rho^2} = \frac{\rho}{\Omega}, \quad d\mu = \frac{d\rho}{\Omega}.$$

The conformal metric $g = \Omega^2 \eta$ becomes

$$g = -\Omega^2 d\tau^2 - 2\rho d\rho d\tau + \sin^2 \nu d\rho^2 + (\rho^2 + \Omega^2 \sin^2 \nu) d\nu^2 + \rho^2 \sin^2 \nu d\phi^2.$$

The qualitative behavior of this metric near infinity is similar to the conformal Minkowski metric given in (34); the only difference is the coordinate representation. Therefore we conclude that hyperboloidal compactification of suitable hyperbolic equations in prolate spheroidal coordinates leads to regular equations as for spherical or oblate spheroidal coordinates.

It is not clear currently whether the method can be applied using Cartesian or cylindrical coordinates. The open question is how to ensure regularity of the equations at corners and edges with respect to limits to infinity. We leave this question for future research.

4. Numerical experiments

An essential advantage in numerical applications of hyperboloidal compactification is the flexibility in the choice of coordinates. An arbitrary coordinate system can be employed in an interior domain, whereas compactification is restricted to a layer outside that domain. This idea is based on the matching method presented in [6]. Numerical applications of the matching method have been difficult in the past due to a blueshift in frequency in the matching region and a large number of free parameters for the transition functions [17, 18, 19].

Hyperboloidal layers discussed in this paper give sufficiently smooth time surfaces without transition functions. However, the layer, although transparent on the analytical level, causes numerical reflections. We compare the numerical accuracy of solutions with and without the layer in one dimension. In three dimensions we focus on the application of hyperboloidal layers. Calculations using hyperboloid foliations, that is, constant mean curvature surfaces without the layer, have been presented in [19].

4.1. One spatial dimension

4.1.1. The analytical setup

Consider the Maxwell equations (26). Assume that the electric permittivity and the magnetic permeability are constant and have unit value. Then the Maxwell system for the unknown vector $\mathbf{u} = (\bar{E}, \bar{H})^T$ reads

$$\partial_\tau \mathbf{u} = -\frac{\Omega^2}{(1-H^2)L} \begin{pmatrix} H & 1 \\ 1 & H \end{pmatrix} \partial_\rho \mathbf{u}. \quad (36)$$

The characteristic speeds are $c_\pm = -\Omega^2/((\pm 1 + H)L)$. This system is similar to the wave equation written in first order symmetric hyperbolic form (25), so our results apply both to Maxwell and wave equations in one dimension.

We experiment with two sets of choices for the compress and heighten functions. First we employ the hyperboloid foliation everywhere in the simulation domain. We set as in (19)

$$\Omega = \frac{S^2 - \rho^2}{2CS} \quad \text{and} \quad H = \frac{2S\rho}{S^2 + \rho^2}.$$

The parameter C controls the coordinate speed of characteristics. They become $c_\pm = \pm(S \pm \rho)^2/(2CS)$. The minus sign corresponds to the incoming speed at the right boundary. It vanishes at $\rho = S$ as expected. The incoming speed at the left boundary corresponds to the plus sign and it vanishes for $\rho = -S$. The qualitative behavior of the characteristics is the same as depicted on the right panel of figure 5. The time step in an explicit time integration scheme is restricted by the maximum characteristic speed. In our case the maximum speed reads $2S/C$. To avoid very small time steps we choose $C = S$ in our numerical experiments.

The second set of compress and heighten functions are chosen for hyperboloidal layers. We set the compress function as in (28)

$$\Omega = 1 - \frac{(\rho - R)^2}{(S - R)^2} \Theta(\rho - R).$$

We determine the heighten function from the requirement of unit outgoing characteristic speeds through the layers. We set

$$H = 1 - \frac{\Omega^2}{L} \quad \text{for } \rho > R, \quad \text{and} \quad H = -1 - \frac{\Omega^2}{L} \quad \text{for } \rho < -R.$$

The characteristic structure for the resulting equations are depicted in figure 7.

4.1.2. The numerical setup

The hyperboloidal method is essentially independent of numerical implementation. We discretize (36) employing common methods. We use an explicit fourth order Runge Kutta time integrator and finite differencing in space with 4th, 6th, and 8th order accurate centered operators. At the boundaries we apply one sided stencils of the same order as the inner operator.

We compare the numerical implementation with and without artificial dissipation. We use Kreiss-Oliger type artificial dissipation to suppress numerical high-frequency waves [20]. For a $2p - 2$ accurate scheme we choose a dissipation operator D_{diss} of order $2p$ as

$$D_{\text{diss}} = \epsilon (-1)^p \frac{h^{2p-1}}{2^p} D_+^p D_-^p,$$

where h is the grid size, D_{\pm} are the forward and backward finite differencing operators and ϵ is the dissipation parameter.

Both for the hyperboloid foliation and the layer we set $S = 10$. The simulation domain is then given by $\rho \in [-10, 10]$. It corresponds to the unbounded domain $x \in (-\infty, \infty)$. The interface for the layer is at $R = \pm 5$. The layer is constructed such that within the domain $|\rho| < 5$, hyperboloidal coordinates (ρ, τ) coincide with standard coordinates (x, t) .

We solve the initial value problem for (36) with a Gaussian wave packet centered around the origin for the electric field and vanishing data for the magnetic field. We set at the initial time surface

$$\bar{E}(\rho, 0) = e^{-\rho^2}, \quad \bar{H}(\rho, 0) = 0.$$

We emphasize that the constructed solutions using the hyperboloid foliation and the hyperboloidal layer correspond to different initial value problems due to the different time surfaces. The solution constructed using the hyperboloidal layer corresponds, however, to the solution that one would obtain using the standard coordinates (x, t) .

4.1.3. The results

Figure 10 shows convergence factors for the electric field from a three level convergence test with 100, 200, and 400 grid cells. The convergence factor is measured for the electric field in the L_2 norm and is calculated by $Q := \log_2 \frac{\|E^{low} - E^{med}\|}{\|E^{med} - E^{high}\|}$. The measured factors are in accordance with the implemented finite difference operators.

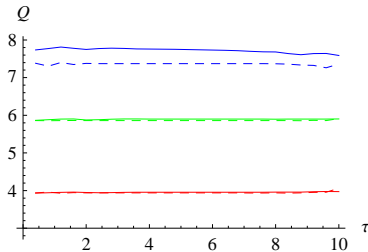


Figure 10: Convergence factors in time in the L_2 norm for the Maxwell equations in one space dimension. Solid curves represent the hyperboloid foliation, dashed curves the layer method. The curves indicate from bottom to top 4th, 6th, and 8th order convergence in accordance with the order of implemented finite differencing operators.

By Huygen's principle for Maxwell equations in flat spacetime energy is completely radiated to infinity leaving the zero solution behind. A good measure of the quality of the boundary treatment in such a simulation is the value of the unknown after the initial wave packet leaves the simulation domain. This value is related to the numerical reflection coefficient of the boundary. In our case, the analytical reflection coefficients at the interfaces and at the boundaries are zero.

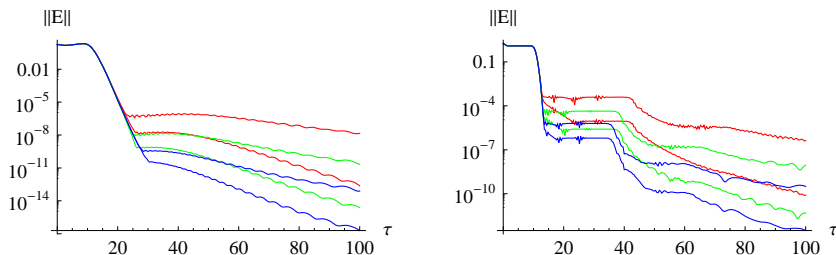


Figure 11: The L_2 norm of the electric field in time for 4th (red), 6th (green), and 8th (blue) order finite differencing with respect to the hyperboloid foliation (left) and the hyperboloidal layer (right). The curve indicating smaller errors to each order corresponds to the solution with artificial dissipation. The plot shows that the effect of dissipation to the quality of the solution is comparable to using a higher order numerical discretization. Errors with the layer method are larger than errors with the hyperboloid foliation due to numerical reflections at the interface.

Numerically, however, it can be expected that the interfaces and the finite differencing at the outer boundaries cause reflections. To measure these reflections we plot the L_2 norm of the solution as a function of time in figure 11.

The plot on the left depicts the field for the hyperboloid foliation, the one on the right for the layer. The errors are larger for the layer as expected. Red, green, and blue curves represent solutions calculated with 4th, 6th, and 8th accurate finite difference operators respectively. To each order we calculate the solution with and without dissipation. Artificial viscosity reduces numerical errors strongly. Its effect to the quality of the solution is similar to using a higher discretization method. Figure 11 shows that the error at late times with 4th order stencils with dissipation has the same order of magnitude as the one with 8th order stencils without dissipation.

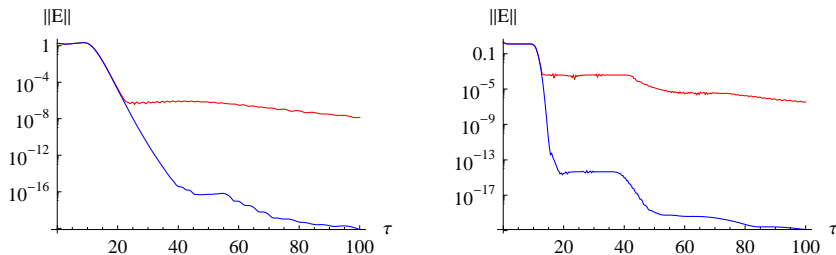


Figure 12: Comparison of numerical errors as indicated by late time values of the L_2 norm of the electric field between a numerical solution with low (red) and high accuracy (blue) for the hyperboloid (left) and the layer (right) method. Accuracy with hyperboloidal compactification is not restricted by the boundary treatment.

The main result from figures 10 and 11 is that the numerical error can be reduced by using higher resolution, higher order discretization, and artificial viscosity. The boundary treatment does not introduce errors into the solution that are put in by hand. To emphasize this point, we plot in figure 12 two solutions using the hyperboloid foliation and the layer method. For each method, one solution is obtained with 4th order finite differencing, without dissipation, and 100 grid cells (red curve); the other solution is obtained with 8th order finite differencing, with dissipation, and 200 grid cells (blue curve). The combined effect of these improvements demonstrates that accuracy with hyperboloidal compactification is not restricted by the boundary treatment but by the numerical accuracy in the simulation domain.

4.2. Three spatial dimensions

In this section we present a numerical implementation of hyperboloidal layers for the scalar wave equation in three spatial dimensions. We apply the conformal method to the scalar wave equation as in section 3.2. Tests with constant mean curvature foliations can be found in [19].

4.2.1. The analytical setup

Consider the wave equation with a focussing power nonlinearity, $\square_\eta u = -u^p$. To construct solutions to this equation, we solve the conformal scalar wave equation

$$\square_g v = \frac{1}{6} R[g] v - \Omega^{p-3} v^p, \quad (37)$$

where g is the conformal metric, $R[g]$ is the Ricci scalar to the metric g , and $v = \Omega^{-1}u$. The conformal metric g is obtained from the Minkowski metric η given in (33) by the time transformation $\tau = t - h(r)$, the spatial compactification $r = \rho/\Omega$, and the conformal rescaling $g = \Omega^2\eta$. We choose the conformal factor Ω such that it is unity in a compact domain bounded by radius R , the coordinate location of the interface, and such that it approaches zero towards the outer boundary located at S , the coordinate location of infinity. We set

$$\Omega = 1 - \left(\frac{\rho - R}{S - R}\right)^4 \Theta(\rho - R), \quad L = 1 + \frac{(\rho - R)^3(3\rho + R)}{(S - R)^4} \Theta(\rho - R).$$

This choice leads to a continuous Ricci scalar at the interface. The heighten function is chosen such that the outgoing characteristic speed through the layer is unity (30). The conformal metric becomes

$$g = -\Omega^2 d\tau^2 - 2(L - \Omega^2) d\tau d\rho + (2L - \Omega^2) d\rho^2 + \rho^2 d\sigma^2.$$

For $\rho < R$ we recover the Minkowski metric (33). The characteristic speeds of spherical wave fronts are

$$c_{\pm} = \frac{L \pm L - \Omega^2}{2L - \Omega^2}.$$

The outgoing speed is of spherical wave fronts unity everywhere, and the incoming speed vanishes at infinity, but is unity inside the domain $\rho < R$. The characteristic structure is similar to the right half of figure 7. The Ricci scalar reads

$$R[g] = \frac{6\Omega(\Omega L' - 2L\Omega')}{\rho^2 L^3}.$$

The apostrophe denotes the derivative by the argument.

4.2.2. The numerical setup

We apply similar numerical techniques as those that have been used to test constant mean curvature foliations presented in [19]. A current requirement for the application of the hyperboloidal method is a spherical grid boundary. We use a code that can handle spherical boundaries called the Spectral Einstein Code (SpEC) [21]. Spatial derivatives are discretized by a pseudospectral method: Chebyshev polynomials in the radial direction, spherical harmonics in the angular directions. Time integration is performed with a Runge-Kutta algorithm. The scalar wave equation is written in first order symmetric hyperbolic form. Characteristic information is exchanged between the subdomains. The numerical grid consists of an inner cube around the origin and spherical shells extending to a spherical outer boundary that corresponds to infinity as depicted in figure 13 (see [19] for details).

Our simulation domain in the radial direction is given by $\rho \in [0, 20]$. The domain structure includes a cube around the origin with the domain $x_i \in [-2, 2]$ and 4 spherical shells extending to future null infinity (figure 13). The interface to the layer is located at $R = 10$. There is no specific reason for setting the

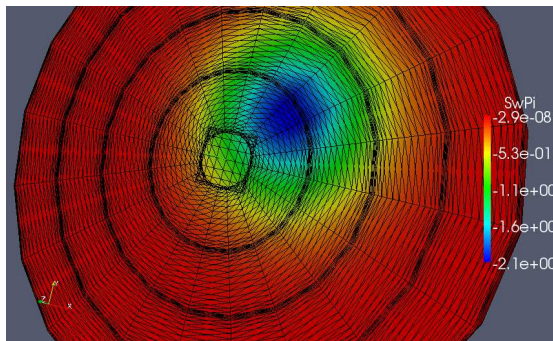


Figure 13: The numerical grid for calculations in Minkowski spacetime. We have a cube around the origin with the domain $[-2, 2]$ in each Cartesian direction and 4 spherical shells extending from $\rho = 2$ to future null infinity at $\rho = 20$. The colors depict off-centered Gaussian initial data for the time derivative of the scalar field.

interface at $R = 10$. Future research should determine how the width of the hyperboloidal layer effects numerical accuracy of the calculations. The colors in figure 13 depict the off-centered data prescribed for the time derivative of the scalar field. The data for the scalar field vanishes.

4.2.3. The results

Spatial truncation errors converge exponentially in a pseudospectral code. We show such spectral convergence in figure 14 for an evolution with vanishing source and off-centered initial data as measured by the L_2 -norm of the constraint field

$$C_i = v_i - \partial_i v, \quad (38)$$

in time. Each curve corresponds to an evolution with N collocation points in each direction (radial and angular directions in the shells, Cartesian directions in the cube around the origin). The constraint error grows slowly in time but the evolution is stable. Convergence is not disturbed by the presence of the boundary located at $\rho = 20$.

A stringent test for boundary methods is the inclusion of nonlinear terms in the equations. The boundary treatment for semilinear wave equations is a difficult problem, especially in three spatial dimensions [3]. Therefore, we present results from the wave equation with a cubic power nonlinearity as a source term. We set $p = 3$ in (37). There is backscatter due to self interaction of the field violating Huygen's principle. Transparency boundary conditions must not eliminate all reflections from the outer boundary but only spurious ones. This makes the treatment of the boundary difficult within the artificial outer boundary problem.

The backscatter by the nonlinear term leads to a late time polynomial decay of the solution. The field at late times decays as t^{-2} at a finite distance from the origin. The rescaled field at infinity decays as t^{-1} . It is difficult to obtain the correct decay rate at a finite distance with an artificial outer boundary.

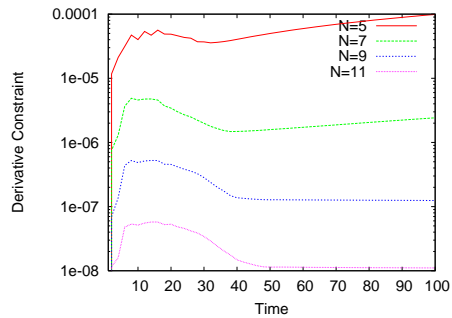


Figure 14: Spectral convergence for the evolution of off-centered initial data in Minkowski spacetime by the L_2 norm of the constraint fields C_i (38).

The decay rate at infinity is not even accessible with standard methods. Figure 15 shows that both rates can be calculated accurately with the hyperboloidal method. The local decay rate is defined as $d \ln |v(\rho, \tau)| / d \ln \tau$. The invariance of the time direction under hyperboloidal transformations implies that the decay rates calculated with the hyperboloidal method are equivalent to the decay rates calculated with the untransformed equations.

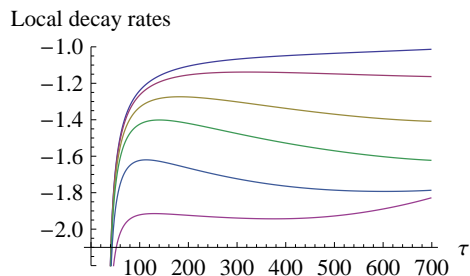


Figure 15: Local decay rates for the cubic wave equation measured by observers located from top to bottom at $\rho = \{20, 19.97, 19.9, 19.8, 19.4, 17.86\}$, or equivalently at $r = \{\infty, 1970, 500, 226, 87, 29\}$. The bottom curve that corresponds to the fastest decay bends up after $\tau = 500$ due to accumulation of numerical errors.

Any numerical method fails after a certain time due to accumulation of numerical errors. In figure 15 the bottom curve that corresponds to the fastest decay bends up after about $\tau = 500$. This behavior is expected, and is due to accumulated numerical errors. We can delay its appearance by increasing the numerical resolution of the simulation. This suggests that the long time accuracy of the solution is not limited by the location of the boundary or the order of boundary conditions, but solely by the accuracy of the interior calculation.

5. Discussion

Hyperboloidal compactification provides a clean solution to the artificial outer boundary problem in certain cases by allowing us to solve suitable hyperbolic equations numerically on unbounded domains. It originates in studies of asymptotic structure of spacetimes in general relativity [4, 5]. It is remarkable that such a practical method can be derived from the interface between differential geometry, conformal structure, partial differential equations, and numerical analysis.

With the hyperboloidal layer method, in which compactification is restricted to a layer, we can apply arbitrary coordinates in an interior domain, and we have quantitative access to the asymptotic solution. The numerical boundary of the simulation domain corresponds to infinity, and therefore no outer boundary conditions are needed. The hyperboloidal time transformation leads to a non-vanishing coordinate speed for outgoing characteristics up to and including infinity with respect to compactifying coordinates.

Some further advantages of the hyperboloidal method are as follows. The wavelength of outgoing radiation can be influenced by free parameters, which can be used to improve efficiency of numerical calculations. The transformations can be applied in a straightforward manner to various covariant hyperbolic equations, such as wave, Maxwell, or Yang-Mills equations. Inclusion of source terms and nonlinearities poses no difficulties as long as certain asymptotic fall-off conditions are satisfied. Calculation of boundary data that depends on the particular system of equations is not necessary. The boundary treatment introduces no errors, therefore no error controlling is needed. There is no overhead in software implementation of boundary routines. The geometric nature of the method makes it largely independent of numerical schemes.

The disadvantages of the method should be studied in future research. An important current limitation is the requirement of spherical or spheroidal grids near the outer boundaries. It is not clear whether hyperboloidal compactification can be performed using Cartesian or cylindrical coordinates, which require a stable numerical treatment of corners and edges. Another interesting question is whether the method can be extended to non-covariant problems, or problems including infinitely extended matter fields, such as anisotropic elastic waves, optical waveguides, or Euler equations.

The decision whether to apply hyperboloidal compactification or not can only be made after detailed comparative studies. In this context, it would be interesting to compare the hyperboloidal method with other approaches to the outer boundary problem, such as absorbing boundary conditions or perfectly matched layers.

The idea of boosting the time direction for certain purposes may find applications other than compactification. It seems that transformations of the characteristic cone for hyperbolic equations has been left largely unexplored outside numerical relativity. The presented solution of the outer boundary problem may be just one application of such transformations. Others might be useful, for example in numerical studies of high frequency waves.

Acknowledgments

I thank Daniel Appelö, Eliane Bécache, and Frédéric Nataf for discussions, Larry Kidder for his help with SpEC, and Piotr Bizoń, Philippe LeFloch, and Eitan Tadmor for support. This research was supported by the National Science Foundation (NSF) grant 07-07949 in Maryland, by the Marie Curie Transfer of Knowledge contract MTKD-CT-2006-042360 in Kraków, and by the Agence Nationale de la Recherche (ANR) grant 06-2-134423 entitled "Mathematical Methods in General Relativity" in Paris.

References

- [1] D. Givoli, High-order local non-reflecting boundary conditions: A review, *Wave Motion. New computational methods for wave propagation* 39 (2004) 319–326.
- [2] T. Hagstrom, S. Lau, Radiation boundary conditions for Maxwell’s equations: A review of accurate time-domain formulations, *Journal of Computational Mathematics* 25 (2007) 305–336.
- [3] J. Szeftel, A nonlinear approach to absorbing boundary conditions for the semilinear wave equation, *Math. Comp.* 75 (2006) 565–594.
- [4] R. Penrose, Asymptotic properties of fields and space-times, *Phys. Rev. Lett.* 10 (1963) 66–68.
- [5] H. Friedrich, Cauchy problems for the conformal vacuum field equations in general relativity, *Comm. Math. Phys.* 91 (1983) 445–472.
- [6] A. Zenginoglu, Hyperboloidal foliations and scri-fixing, *Class. Quant. Grav.* 25 (2008) 145002. arXiv:0712.4333, doi:10.1088/0264-9381/25/14/145002.
- [7] J.-P. Bérenger, A perfectly matched layer for the absorption of electromagnetic waves, *J. Comp. Phys.* 114 (1994) 185–200.
- [8] W. C. Chew, W. H. Weedon, A 3D perfectly matched medium from modified Maxwell’s equations with stretched coordinates, *Microwave and Optical Technology Letters* 7 (1994) 599–604.
- [9] S. Abarbanel, D. Gottlieb, A mathematical analysis of the PML method, *J. Comp. Phys.* 134 (1997) 357–363.
- [10] D. Appelö, T. Hagstrom, G. Kreiss, Perfectly matched layers for hyperbolic systems: General formulation, well-posedness, and stability, *SIAM Journal on Applied Mathematics* 67 (1) (2006) 1–23.
- [11] E. Bécache, S. Fauqueux, P. Joly, Stability of perfectly matched layers, group velocities and anisotropic waves, *J. Comp. Phys.* 188 (2003) 399–433.

- [12] R. M. Wald, *General relativity*, The University of Chicago Press, Chicago, 1984.
- [13] R. Penrose, Zero rest-mass fields including gravitation: Asymptotic behaviour, *Proc. Roy. Soc. Lond. A*284 (1965) 159–203.
- [14] R. Geroch, Asymptotic structure of space-time, in: F. Esposito, L. Witten (Eds.), *Asymptotic Structure of Space-Time*, Plenum Press, 1977, pp. 1–105.
- [15] H. Friedrich, Conformal Einstein evolution, *Lect. Notes Phys.* 604 (2002) 1–50. arXiv:gr-qc/0209018.
- [16] A. Zenginoglu, A hyperboloidal study of tail decay rates for scalar and Yang-Mills fields, *Class. Quant. Grav.* 25 (2008) 175013. arXiv:0803.2018, doi:10.1088/0264-9381/25/17/175013.
- [17] A. Zenginoglu, M. Tiglio, Spacelike matching to null infinity, *Phys. Rev. D*80 (2009) 024044. arXiv:0906.3342, doi:10.1103/PhysRevD.80.024044.
- [18] A. Zenginoglu, Asymptotics of Schwarzschild black hole perturbations, *Class. Quant. Grav.* 27 (2010) 045015. arXiv:0911.2450, doi:10.1088/0264-9381/27/4/045015.
- [19] A. Zenginoglu, L. E. Kidder, Hyperboloidal evolution of test fields in three spatial dimensions, *Phys. Rev. D*81 (2010) 124010. arXiv:1004.0760, doi:10.1103/PhysRevD.81.124010.
- [20] H. O. Kreiss, J. Olinger, *Methods for the approximate solution of time dependent problems*, International Council of Scientific Unions, World Meteorological Organization, Geneva, 1973.
- [21] L. Kidder, H. Pfeiffer, M. Scheel, SpEC: Spectral Einstein Code. URL <http://www.black-holes.org/SpEC.html>